2019 IEEE 16th International Symposium on Biomedical Imaging (ISBI 2019)
Venice, Italy, April 8-11, 2019

3D REGIONAL SHAPE ANALYSIS OF LEFT VENTRICLE USING MR IMAGES: ABNORMAL MYOCADIUM DETECTION AND CLASSIFICATION

Han Bao*[1], Hui Ren*[1,2], Zhiling Zhou[1], Xiang Li[1], Ning Guo[1], Quanzheng Li[1] *Joint first authors

[1] *Department of Radiology, Massachusetts General Hospital and Harvard Medical School*
[2] *Department of Cardiology, Peking University People's Hospital and Peking University Health Science Center*

ABSTRACT

Accurate detection of abnormal myocardium regions is essential for differential diagnosis of cardiovascular disease. However, to achieve this goal by image analysis will significantly increase the burden on radiologists who is already overwhelmed. To ease the time and energy-demanding process and enhance the reproducibility, we proposed a novel framework for automatic abnormal shape detection on left ventricular (LV) using MR images. Our proposed approach utilizes the features obtained by large deformation diffeomorphic metric mapping (LDDMM). To take advantage of 3D structural information, we introduce multilinear principal component analysis (MPCA) in the framework to reduce feature dimensions. Then we combine MPCA with linear discriminant analysis (LDA) to perform differential diagnosis. The performance of proposed framework is evaluated on patients' images. In the classification of three common cardiovascular diseases, our proposed method outperformed traditional classifiers (Global point signature, Random Forest and XGBoost) with an accuracy of 94%. To further automatically detect the dysfunctional heart regions, we did a comparison on 3D morphology between the diseased subjects and healthy controls and performed an automatic visualization of the abnormal myocadiac regions. In conclusion, our proposed framework reserves the spatial information of the features generated through LDDMM registration and enables the 3D visualization of abnormal regions of LV. With the advance of our method, differential diagnosis is successfully performed on patients with different cardiovascular diseases.

Index Terms— Left ventricle, regional shape analysis, 3D, classification, registration.

1. INTRODUCTION

As an estimation, 92.1 million US adults have at least 1 type of Cardiovascular disease (CVD) and the number is still increasing. The relative cost is predicted to be $818 billion annually by 2030 [1]. The recent advances in image-based computational analysis has achieved promising performance in various applications, particularly individual estimation of left ventricular (LV) geometry [2-4]. As a noninvasive imaging modality, cardiac magnetic resonance (CMR) imaging has been widely used and provides details of LV structure in 3-dimension (3D). Combining these advanced tools with regional metrics of LV facilitates automatic detection of abnormal myocardial regions. And it certainly assists to identify patients with high risk of CVD or poor prognosis.

In image analysis, the optimal index to detect abnormal myocardium remains unclear. Previous studies have indicated that several indices describing regional morphology, such as wall thickness, strain and curvature. On one hand, these indices are usually correlated to the AHA 17-segment model and only suitable for ischemic heart disease. Thus, the variance among the standard template and individual heart shape limits the application in clinical diagnosis and disease evaluation [5-6]. On the other hand, given the deformation could be heterogeneous even within one segment of myocardium, using one index to represent a segment seems arbitrary. Thus, the shape changes presented in 17-segment model is incapable to describe accurate myocardium deformation, and sometimes even results in misunderstanding. Therefore, adopting more elaborated pixel-level shape analysis is reasonable for precised diagnosis, risk stratification and therapeutic management.

To study the 3D shape variance among diseased groups, registration has to be completed as first step and determined the validity of further model evaluation. Large deformation diffeomorphic metric mapping (LDDMM), a comprehensive framework for 3D shape registration, has demonstrated its effectiveness in the context of computational anatomy, such as brain, heart, and fiber bundles [7-8]. The features yielded by registration are useful since they decode pixel-wised shape deformation. Previous work has employed linear discriminant analysis (LDA) and other machine learning classifiers with flattened LDDMM features to classify multiple cardiac dysfunctional groups [9]. However, the original features produced by LDDMM containing spatial information is eliminated by flattening. Thus, developing a classification method that preserves 3D geometric information resided in features becomes of great significance.

The primary goal of this study is to propose a novel framework that helps to automatically extract regional 3D indices representing abnormal LV morphology. Multilinear principal component analysis (MPCA) and linear discriminant analysis (LDA) were used together to complete this task. Hence, 3D spatial structural information derived from shape features can be successfully preserved. In this study, we evaluate the performance of proposed framework in disease classification among myocardial infarction, hypertrophic cardiomyopathy and heart failure and further detect patient-specific abnormal myocardium regions.

978-1-5386-3640-4/19/$31.00 ©2019 IEEE

2. METHOD

2.1. Data Acquisition

Our study included 24 subjects from Sunnybrook Cardiac Data. Three different types of common heart diseases are included in the dataset, such as heart failure with myocardial infarction (HFI), heart failure without infarction (HFNI) and hypertrophy (HYP) patients. The characteristics of 24 patients are summarized in Table 1. There are 8 subjects on each group who has underwent CMR test. The cine MR images on standard Steady-state free precession (SSFP) sequence for each patient were obtained. Short and long axis (SAX and LAX) contours at end-of-systolic phase were manually labeled by radiologists. For each subject, there are 2 to 3 ground-truth LAX contours and 8 to 10 SAX contours.

Table 1. Characteristics of patient cohort

	HYP	HFNI	HFI
Male Cases	5	4	5
Age(year)	61(13)	72(12)	55.5(13)
LVEDV (ml)	130 (51)	238(56)	190(41)
LVESV (ml)	37(21)	144(43)	162(52)

HYP: Hypertrophy; HFNI: heart failure without infarction; HFI: heart failure with myocardial infarction; LVEDV: Left ventricular end-diastolic volume; LVESV: Left ventricular end-systolic volume. There are 8 cases in each group. Age, LVEDV, LVESV are reported as mean (standard deviation).

2.2 Reconstruction of 3D Morphology Model

To correct the heart motion due to respiration, SAX contours on MR images were aligned as the first step of 3D cardiac shape construction. The incompressible part referring to interventricular septum of SAX images were matched with the one of the LAX images, as suggested in [10].

Triple-spline interpolation were then conducted to build 3D surface from LAX (vertical, horizontal and three chamber view) and SAX contours. The built surface was convoluted with 3D Gaussian kernel for smoothing. Hausdorff Distance [11] was used as a measurement of the total reconstruction error, which was defined as the sum of Euclidean distance between the ground-truth contours and the newly built 3D surface over all the pixel points on the ground truth contours. The squared errors for each point on the constructed surface is about 0.4mm for epicardium, and 0.25mm for endocardium.

2.3. Registration

Before conducting group-wise comparison, affine registration was performed on constructed surfaces and followed with non-rigid registration using LDDMM. In the affine registration step, central line of LV was defined as the line from endocardial apex to the mitral annular center, which was visually checked with better accuracy in the dataset. Landmarks at the junction of left and right ventricles were used to rotate SAX images into standard orientation. After this, LDDMM-ot method [12] was used to construct a normal template from 8 healthy controls provided by Sunnybrook

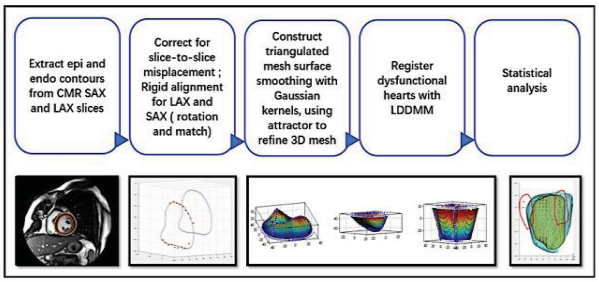

Figure 1. Flow charts of proposed framework.

dataset while multi-kernel LDDMM [13] was used to register all individual 3D models.

2.4. Abnormal Regions Visualization on 3D Surfaces

Multilinear principal component analysis (MPCA) was applied to extract features that mostly contributed to the group differentiation. Those principle features (top 5) were retrieved and projected to the original 3D models for visualization. MPCA is a multilinear extension of PCA on n-way arrays. MPCA performs normal PCA on each of the three axes separately, iterates the process till converge on all the dimensions. For simplicity, we formulated the feature extraction steps on one axis as follows.

$$\textbf{\textit{Decomposition:}}\ \ v_k = argmax(Xv)^T(Xv),$$
$$\text{where } \|v\| = 1,\ v^T v_j = 0, j = 1 \dots k-1$$
$$\textbf{\textit{Reconstruction from the first k features:}}$$
$$X' = Xv_{1\dots k}v_{1\dots k}^T$$

2.5 Disease Classification

After registration, the total length of deformation routine (amplitude of deformation, AOD), as well as the displacement field between the target surface and the points on contours can be calculated. They were viewed as two direct measurements of shape change from source to target during the registration [14]. Using normal template as the deformation source, the displacement field quantify the difference of surface region between template and diseased cases. Therefore, abnormally large changes in shape point to dysfunctional regions. The initial step of the whole deformation process (initial momentum) and the Jacobian matrix (direction controller) between the template and target were also included as features in our classification. These features captured shape changes from different perspectives.

Previous works have reported the use of LDA, random forest and logistic regression in classifying subjects base on LDDMM features [15]. To improve the performance, MPCA was introduced in our classification. In this step, labels were not provided, and the outputs are a set of 3D features which contribute mostly to the group variance. Therefore, the spatial information is preserved and leads to a higher accuracy in the classification.

Features screened by MPCA may not be the ones that best separate different groups since only those features mostly

contributed to group variance were picked. Further selection by LDA was needed. In pair-wise comparison between each two groups, features that minimized the distance within group as well as maximize the distance between groups were chosen. Eventually, these concatenated 3D features construct a vector that served as input in the classification. We used features that could contribute to 30% of the group variance in MPCA. In LDA, the most powerful ten features were selected to differentiate the subjects of each pair of groups. To denote abnormal regions, we used first five components with the same methods as in classification. All steps were illustrated in Figure 1.

3. RESULTS

3.1 Visualization of the Abnormal Regions

The regions that indicate potential abnormal myocardium were visualized in a 3D surface model. In Figure 2, one case in each HYP, HFNI and HFI group were illustrated as examples. In Figure 2 left column, the abnormal regions were highlighted (light blue) on the 3D LV model by projecting the first 5 components mentioned in 2.4. In the bulls-eye diagrams (Figure 2 middle column), the point-level shape changes based on displacement field were summarized and presented according to AHA 17-segment model. Few segments on the endocardium of left ventricle were highlighted with yellow and blue color, referring that these segments were closer or farther to the central line comparing to normal cases, which could also be seen in SAX and LAX images accordingly (right two columns in Figure 2). Meanwhile, the neighbor segments of enlarged areas (in blue) showed a general tendency of more exerted contraction, consisting with morphology compensation in LV remodeling.

The visualization results demonstrated a high concordance between abnormal regions in 3D LV model and abnormal segments. For example, in the HYP case (first row in Figure 2), basal inferior wall (region 4), mid-inferior wall (region 10) and mid-inferolateral wall (region 11) were highlighted on the 3D surface. Moreover, the proposed pixel-wise visualization framework depicted the dysfunctional myocardium in a more elaborated fashion than the bulls-eye diagram. Despite the heterogeneity of the regional variations expected for different patients with given conditions, the major abnormal regions were still reliably indicated.

3.2 Classification Results

The classification results are summarized in table 2. Correlation among features were analyzed within epicardium or endocardium, and between them as well. Results showed that: the correlation between AOD and Jacobian on both epicardium and endocardium were 0.9; the correlation between Initial Momentum and Jacobian on epicardium was 0.41; the correlation between all the other features were lower than 0.20.

The performance of classification for three different heart diseases were summarized in Table 2. Comparing with other common methods, our platform yielded highest accuracy of 94% for all three classification tasks, which significantly outperformed the reference methods including random forest and XGBoost. The improvement on the accuracy of random forest solely was achieved by integrating additional structural information. Whereas adopting a stronger classifier-XGBoost didn't improve the performance of random forest.

To examine the effectiveness of LDDMM-based registration, Global Point Signature, a pipeline completes auto shape registration and classification, was included into comparison as a sensitive analysis [16]. Results suggested that LDDMM-based registration generally yielded a higher accuracy on our dataset.

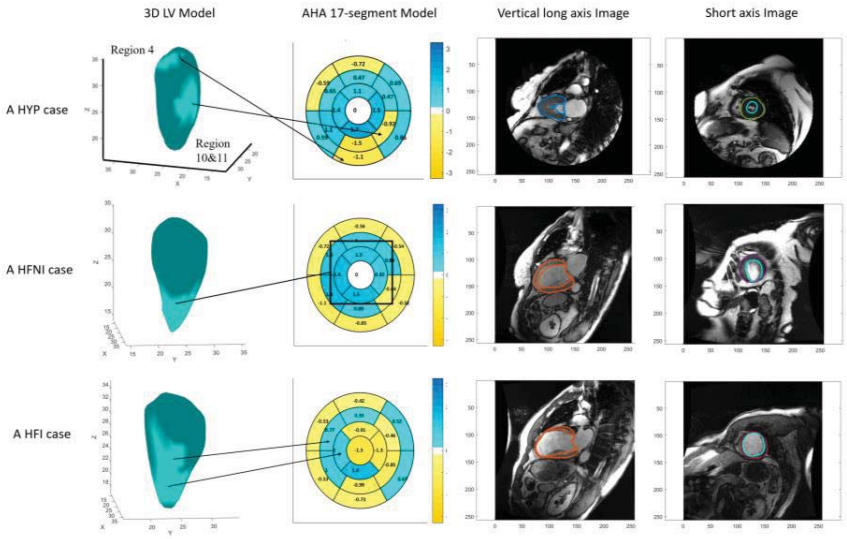

Figure 2. Visualization of abnormal regions on endocardium of left ventricle

Table 2. Classification Results

Task	Methods	Leave-one-out Accuracy (%)	Sensitivity (Specificity) (%)
HFNI vs. HFI	Global Points Signature	68.75	87.50 (50.00)
	Random Forest	62.50	75.00 (50.00)
	XGBoost	75.00	87.50 (62.50)
	MPCA + LDA + Random Forest	94.00	100 (89.00)
HFI vs. HYP	Global Points Signature	62.50	75.00 (50.00)
	Random Forest	62.50	50.00 (75.00)
	XGBoost	62.50	62.50 (62.50)
	MPCA + LDA + Random Forest	94.00	100 (89.00)
HFNI vs. HYP	Global Points Signature	62.50	87.50 (37.50)
	Random Forest	68.75	75.00 (62.50)
	XGBoost	68.75	62.50 (75.00)
	MPCA + LDA + Random Forest	94.00	89.00 (100)

HYP: Hypertrophy; HFNI: heart failure without infarction; HFI: heart failure with myocardial infarction; MPCA: Multilinear principal component analysis; LDA: linear discriminant analysis.

4. CONCLUSION

In this study, a new CMR image-based framework are proposed to classify heart diseases with different etiologies. For leveraging more 3D structural information, the approach combining MPCA and LDA significantly improves classification accuracy, which enables the individual abnormal myocardium to be detected and visualized automatically. Although analysis was conducted within a small dataset at ES, our work showed great potential in disease differential diagnosis, treatment planning, and patient follow-up. Further validation and investigation in larger population with more temporal information should be considered to helping ease the burden of radiologists and improve the effectiveness in clinical setting.

5. ACKNOWLEDGEMENT

This work was supported by the National Institutes of Health under grant RF1AG052653, P41EB022544 and C06 CA059267.

REFERENCES

[1] E. J. Benjamin et al., "Heart Disease and Stroke Statistics—2017 Update," Circulation, vol. 135, pp. e146–e603, Mar. 2017.

[2] J. H. Thrall et al., "Artificial Intelligence and Machine Learning in Radiology: Opportunities, Challenges, Pitfalls, and Criteria for Success," J Am Coll Radiol, vol. 15, no. 3 Pt B, pp. 504–508, 2018.

[3] F. Vadakkumpadan, et al., "Image-based left ventricular shape analysis for sudden cardiac death risk stratification," Heart Rhythm, vol.11, pp.1693–1700, Oct. 2014.

[4] E.-Y. Choi et al., "Prognostic value of myocardial circumferential strain for incident heart failure and cardiovascular events in asymptomatic individuals: the Multi-Ethnic Study of Atherosclerosis," Eur Heart J, vol. 34, no. 30, pp. 2354–2361, Aug. 2013.

[5] M. D. Cerqueira et al., "Standardized Myocardial Segmentation and Nomenclature for Tomographic Imaging of the Heart," Journal of Cardiovascular Magnetic Resonance, vol. 4, no. 2, pp. 203–210, 2002.

[6] J. Jung, Y.-H. Kim, N. Kim, and D. H. Yang, "Patient-specific 17-segment myocardial modeling on a bull's-eye map," 453–465, Sep. 2016.

[7] S. Ardekani et al., "Computational Method for Identifying and Quantifying Shape Features of Human Left Ventricular Remodeling" Ann Biomed Eng, vol.37, pp.1043–1054, Jun. 2009.

[8] K. Oishi et al., "Atlas-based whole brain white matter analysis using large deformation diffeomorphic metric mapping: Application to normal elderly and Alzheimer's disease participants," NeuroImage, vol. 46, pp. 486–499, Jun. 2009.

[9] J. Feng, X. Tang, M. Tang, C. Priebe, and M. Miller, "Metric Space Structures for Computational Anatomy," in Machine Learning in Medical Imaging, 2013, pp. 123–130.

[10] B. Villard, E. Zacur, E. Dall'Armellina, and V. Grau, "Correction of Slice Misalignment in Multi-breath-hold Cardiac MRI Scans," in Statistical Atlases and Computational Models of the Heart. Imaging and Modelling Challenges, 2017, pp. 30–38.

[11] N. Aspert, D. Santa-Cruz, and T. Ebrahimi, "MESH: measuring errors between surfaces using the Hausdorff distance," in Proceedings. IEEE International Conference on Multimedia and Expo, 2002, vol. 1, pp. 705–708 vol.1.

[12] M. Descoteaux, L. Maier-Hein, A. Franz, P. Jannin, D. L. Collins, and S. Duchesne, Medical Image Computing and Computer-Assisted Intervention − MICCAI 2017: 20th International Conference, Quebec City, QC, Canada, September 11-13, 2017, Proceedings. Springer, 2017.

[13] L. Risser, F.-X. Vialard, R. Wolz, D. D. Holm, and D. Rueckert, "Simultaneous Fine and Coarse Diffeomorphic Registration: Application to Atrophy Measurement in Alzheimer's Disease," in Medical Image Computing and Computer-Assisted Intervention – MICCAI 2010, pp. 610–617.

[14] L. Risser, F. Vialard, R. Wolz, M. Murgasova, D. D. Holm, and D. Rueckert, "Simultaneous Multi-Scale Registration Using Large Deformation Diffeomorphic Metric Mapping," IEEE Transactions on Medical Imaging, vol. 30, no. 10, pp. 1746–1759, Oct. 2011.

[15] L. Wang et al., "Large Deformation Diffeomorphism and Momentum Based Hippocampal Shape Discrimination in Dementia of the Alzheimer type," IEEE Transactions on Medical Imaging, vol. 26, no. 4, pp. 462–470, Apr. 2007.

[16] A. J. Chaudhari, R. M. Leahy, B. L. Wise, N. E. Lane, R. D. Badawi, and A. A. Joshi, "Global point signature for shape analysis of carpal bones," Phys. Med. Biol., vol. 59, no. 4, p. 961, 2014.